PCCP

Accepted Manuscript

ROYAL SOCIETY OF CHEMISTRY

www.rsc.org/pccp

PCCP

PAPER

Reactive oxygen species formed in organic lithium-oxygen batteries†

Received 00th January 20xx,

Accepted 00th January 20xx

DOI: 10.1039/x0xx00000x

www.rsc.org/

Patrick Schwager[a,b], Saustin Dongmo[a], Daniela Fenske[b] and Gunther Wittstock[a]*

Li-oxygen batteries with organic electrolytes are of general interest because of their theoretically high gravimetric energy density. Among the great challenges for this storage technology is the generation of reactive oxygen species such as superoxides and peroxides that may react with the organic solvent molecules and other cell components. The generation of such species has been assumed to occur during the charging reaction. Here we show that superoxide is formed also during the discharge reaction in lithium ion-containing dimethyl sulfoxide electrolytes and is released into the solution. This is shown independently by fluorescence microscopy after reaction with the selective reagent 4-chloro-7-nitrobenzo-2-oxa-1,3-diazole and by local detection using a microelectrode of a scanning electrochemcial microscope positioned in a defined distance of 10 to 90 µm above the gas diffusion electrode.

1. Introduction

Rechargeable Li-oxygen cells with organic electrolytes are considered as an ultimate future storage technology mainly because of its very high theoretical gravimetric energy density of 3842 mA h g^{-1} (considering only the active mass in the discharged state).[1] This calculation is based on the cell reactions

$$2\ Li \rightleftharpoons 2\ Li^+ + 2\ e^- \quad (1)$$

$$O_2 + 2\ e^- + 2\ Li^+ \rightleftharpoons Li_2O_2 \quad (2)$$

Ideally, the charging reaction would proceed as the reversal of reactions (1) and (2). However, the several groups showed that the charging and discharging reaction lead to a broad spectrum of electrolyte decomposition products.[2-6] For instance, ethers,[2-4] carbonates,[5, 7] and sulfoxides like dimethyl sulfoxide (DMSO)[6, 8] decompose during oxygen evolution reaction (OER) which has been explained by the reaction of those solvents with intermediate superoxide $O_2^{\bullet-}$ formed by reaction (3).[9, 10]

$$Li_2O_2 \rightarrow O_2^{\bullet-} + 2\ Li^+ \quad (3)$$

$O_2^{\bullet-}$ is also the typical product of the oxygen reduction reaction (ORR) in organic solution if they are free of proton sources and metal cations such as Li^+.[11, 12]

$$O_2 + e^- \rightarrow O_2^{\bullet-} \quad (4)$$

If a proton source or Li^+ is present, $O_2^{\bullet-}$ rapidly disproportionates according to Eq. (5).

$$2\ O_2^{\bullet-} + 2\ Li^+ \rightarrow O_2 + Li_2O_2 \quad (5)$$

Disproportionation reactions are known to be catalyzed homogeneously or heterogeneously especially in aqueous and biological systems.[13, 14] This offers in principle possibilities to influence intermediate concentration by the solution composition and the design of the electrode material. A recent study of Peng et al. provided evidence of stable $O_2^{\bullet-}$ adsorbates on a polycrystalline Au electrode surfaces even in the presence of a proton source.[15] Apart from this, the generation of $Li_2O_{2(solv)}$ in the solution may lead to oversaturated solutions and precipitation of solid $Li_2O_{2(s)}$ on surfaces.

$$Li_2O_2(solv) \rightleftharpoons Li_2O_2(s) \quad (6)$$

Currently it is unknown to which extend, $O_2^{\bullet-}$ (or derived species such as the ion pair with Li^+, $LiO_2^{\bullet}$) may be formed as intermediates according to equations (4) and (7) that may react with the electrolyte or carbon electrode material before entering into further oxidation (during charging), reduction (during discharging) or disproportionation reactions.

$$Li^+ + O_2^{\bullet-} \rightarrow LiO^{\bullet} \quad (7)$$

Even in alkaline aqueous solution $O_2^{\bullet-}$ has been detected in solution.[16] Our previous study on the detection of oxygen ingress into an Li-oxygen cell by positionable microelectrodes (MEs) indicated an yet unidentified soluble reaction intermediate released during oxygen reduction in Li^+-containing DMSO at a porous carbon electrode.[17] The

[a] Carl von Ossietzky University, Faculty of Mathematics and Natural Sciences, Center of Interface Science, Institute of Chemistry, D-26111 Oldenburg, Germany , email: gunther.wittstock@uni-oldenburg.de
[b] Fraunhofer Institute for Manufacturing Technology and Advanced Materials IFAM, Wiener Straße 12, D-28359 Bremen, Germany

† Supplementary information is available about accumulation of dissolved species at the ME over longer time. See DOI:

experimental setup (Fig. 1) uses a ME at defined, yet fixed position to detect oxygen species in different working modes.

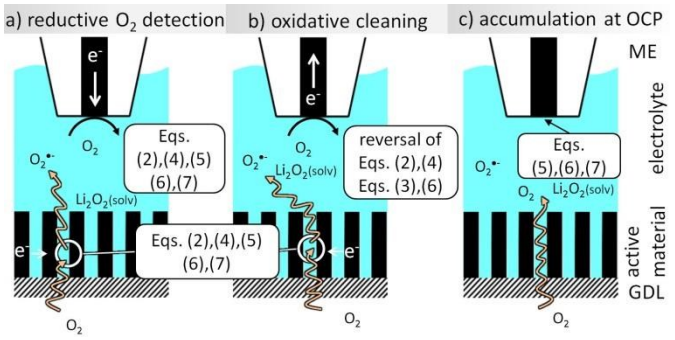

Fig. 1 Scheme of reactions at the ME and GDE.

During ORR at the GDE, the ME performs as well ORR to detect the decrease of dissolved O_2 above the GDE (redox competition mode of SECM, Fig. 1a). In Li^+-containing electrolytes, the electrode surface passivates and can be cleaned by a short oxidative pulse. Here deposited Li_2O_2 will be oxidized (reversal of Eq. (2)). In addition, we found another intermediate that is oxidized while ORR proceeds at the GDE (Fig. 1b). Here we identify this intermediate as $O_2^{\bullet-}$ by reaction with a selective fluorogenic dye and investigate its amount by voltammetry at the ME after accumulation of the compound at OCP (Fig. 1c). By this we prove that this compound (or its ion pair with Li^+) is transported through solution rather than being present only as an adsorbate on the GDE surface.

2. Experimental

2.1 Chemicals

DMSO (98% purity, Carl Roth GmbH, Karlsruhe, Germany) was deaerated and dried for at least 48 h over a 3 Å molar sieve. A solution from 1 M $LiClO_4$ (≥ 99.9 % purity, Sigma Aldrich, Steinheim, Germany) in dried DMSO was prepared inside an Ar-filled glovebox. 4-chloro-7-nitrobenzo-2-oxa-1,3-diazole (NBD-Cl) was purchased from Sigma (≥ 98 % purity, Sigma Aldrich, Steinheim, Germany).

2.2 Electrodes

Pt MEs were produced by sealing a Pt wire of 50 µm diameter (Goodfellow Cambridge Ltd., Huntigdon, England) with a laser-heated micropipette puller (P-2000, Sutter Instruments, Novato, USA) in borosilicate glass capillaries. The assembly was successively polishing in an aqueous suspension of 0.3 µm and 0.05 µm Al_2O_3 particles (MicroPolish II, Buehler, Düsseldorf, Germany). The *RG*-value, i.e. the ratio of outer probe radius r_{glass} = 120 µm (from laser microscopy), and the radius of the active electrode area r_T = 16.9 µm (from the diffusion-limiting current in aqueous 1 mM ferrocenemethanol solution + 0.1 M KNO_3) was *RG* = 7.1. For all measurements a Pt wire auxiliary and an Ag wire quasi-reference electrode were used. All potentials are given with respect to the Ag-QRE.

The gas diffusion electrode (GDE) was prepared from a slurry composed of 4.36 g carbon particles (Vulcan XC R, Worlee-Chemie GmbH, Hamburg, Germany) and 0.68 g binder (Kynar Flex 2801, Tetrachim, Noisiel, France) uniformly dispersed in 45 ml N-methylpyrrolidon (Carl Roth GmbH & Co. KG, Karlsruhe, Germany). The slurry was applied to a carbon paper (Toray™ TP060, Toray Industries, Inc., Tokyo, Japan) by a doctor blade (Erichsen GmbH & Co KG, Hemer, Germany) in a wet thickness of 120 µm. The carbon paper was pre-treated by immersion into a polytetrafluoroethylene suspension (polytetrafluoroethylene preparation, 60 mass-% in H_2O, Sigma–Aldrich, Steinheim, Germany) for 30 s in order to prevent the wetting of the carbon paper by the organic solvent. The GDE was dried in a two-step process (30 min at 80 °C followed by 90 min at 120 °C). For all measurements a Pt wire auxiliary and an Ag wire quasi-reference electrode were used.

2.3 Apparatus and procedures

Superoxide radical formation was monitored after reaction with NBD-Cl by fluorescence using an optical microscope (DM IRE2, inverted configuration, Leica Microsystems GmbH, Wetzlar, Germany) with a HC PL FLUOTAR objective (5×, NA = 0.3, Leica) and a tungsten lamp filtered with a dichroic filter set within the wavelength range of 440-495 nm. Emitted light passing a 515 nm long pass filter was recorded by a DC152QC-FI sCMOS camera (scientific CMOS, Andor Technology, Darmstadt, Germany) attached to the third optical port of the microscope (Fig.Fluorescence 2). The time step setting of the sCMOS was 1 s per frame.

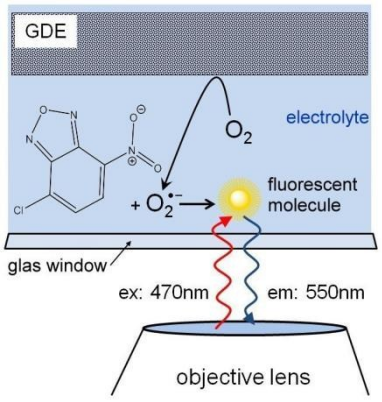

Fig 2 Fluorescence microscopy setup. Oxygen is reduced at the GDE from the oxygen saturated solution (1 M $LiClO_4$, 0.5 mM NBD-Cl in DMSO). The dye selectively reacts with the superoxide to form a fluorescent molecule which is excited at 470 nm wavelengths and emits at 550 nm wavelengths.

The GDE was mounted with the active layer facing downwards. It contacted a 1 mm thick solution layer sandwiched between the GDE and the viewing window. The GDE was connected to a Cu-wire using an electrically conductive epoxy adhesive (EPO-TEK H24, Epoxy Technology Inc., 14 Fortune Drive, Billerica, USA) which was sealed with PDMS. A potentiostat (CH700B, CH Instruments Inc., 3700 Tennison Hill Drive, Austin, USA) in three-electrode configuration was used to drive the oxygen reduction reaction at the GDE in a chronoamperometric experiment while observing the fluorescence emission.

All SECM measurements were performed in a specialized setup described before.[17] It was run under SECMx[18] software and used a positioning system (mechOnics AG, Munich, Germany) and two interconnected Gamry Reference 600 potentiostats acting as a bipotentiostat (Gamry Instruments, Warminster, USA). AC-SECM was used to approach the ME to the GDE surface as described before[19-21] using a frequency of 100 kHz and amplitude of 50 mV. The GDE was left at open circuit potential (OCP). The distance between the ME and GDE was finally determined from the AC measurements and their fits to approach curves of conductive substrates.[22] The measurements were performed in a custom-made chamber containing two different gas reservoirs, one above the GDE and the electrolyte reservoir, one below the GDE. Prior to the experiment both gas chambers were purged with Ar. The Ar flow was sustained at the upper chamber. After dosing in the degassed electrolyte with a syringe through the septum, the lower chamber was continuously purged with a 2 vol.-% O_2 / 98 vol.-% Ar gas mixture at a total flow rate of 100 mL min^{-1} and pressure slightly above 1 bar during the whole experiment.

3. Results and discussion

3.1 Superoxide radical detection by fluorescence microscopy

Superoxide can be indirectly detected via monitoring its reaction products.[23, 24] For instance, after reaction of $O_2^{\bullet-}$ with NBD-Cl, absorbance measurements at 470 nm or fluorescence spectroscopy with excitation at 470 nm and emission at 550 nm wavelengths provide selective detection of $O_2^{\bullet-}$ radicals. This method was used here in combination with a chronoamperometric pulse program applied to the GDE and the spatially and temporally resolved detection of the fluorescence by a CMOS camera. For a better evaluation the background fluorescence from the GDE must be compensated. In order to remove this contribution, the GDE was biased at E_{GDE} = 0 V for 60 s, where no ORR current can be detected. The image taken at t = 60 s was used as a reliable background and was subtracted from all subsequent recordings taken at more negative potentials (Fig. 3). After 60 s the potential was switched to E_{GDE} = -0.7 V for 60 s to cause ORR in the oxygen-saturated electrolyte. The production of $O_2^{\bullet-}$ is evident from the increasing fluorescence intensity recorded between t = 4 s and t = 40 s after the potential step (Fig. 3, panel a)-e)). A control measurement proved that no fluorescent product was formed at E_{GDE} = -0.7 V in an oxygen-free electrolyte (Fig. 3, panel f)). Figure 3g shows the corresponding reflection image recorded after the completion of the fluorescence experiments in solution. One prominent feature has been marked in Fig. 3e and g that allows relocation of a particular point in Fig. 3b-g. The white structures are debris appear only after the solution experiments and could not be removed without detaching flakes of the fragile GDE.

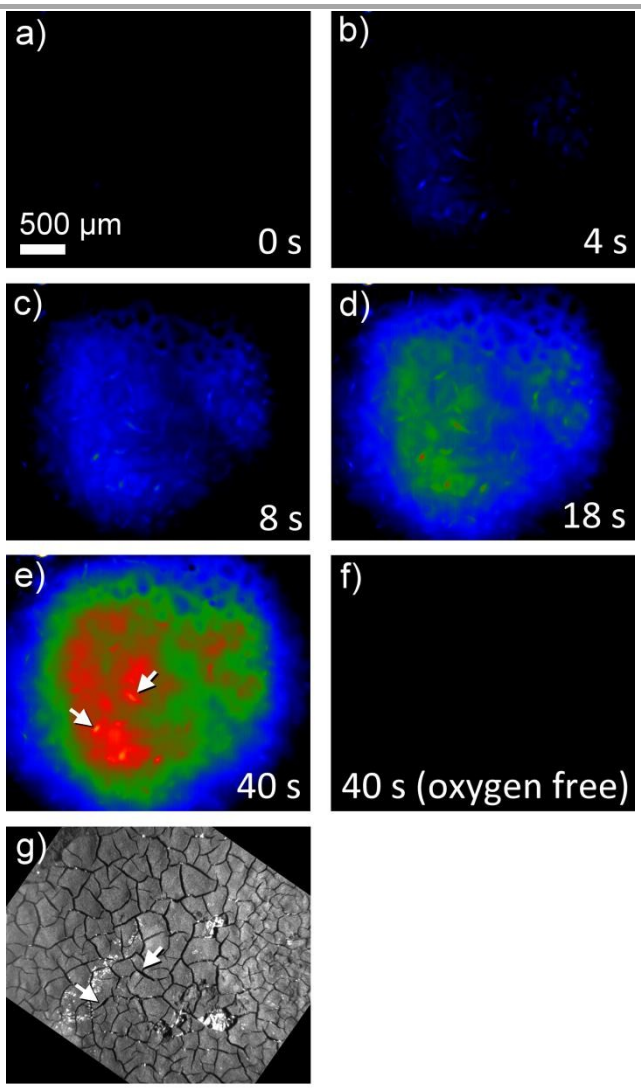

Fig. 3 Fluorescence microscopy image sequence at 0 s at E_{GDE} = 0 V (background) as well as 4 s, 8 s, 18 s and 40 s after the start of an ORR pulse at the GDE (E_{GDE} = -0.7 V). Panel f) shows an image taken after holding the GDE at E_{GDE} = -0.7 V for 40 s in oxygen-free electrolyte solution. The optical focus was set to the GDE surface. Solution was 1 M $LiClO_4$ in DMSO. Panel g is an optical reflection image in the same scale. The marker in panels e) and g) shall aid relocation of specific structures between the fluorescence and reflection images.

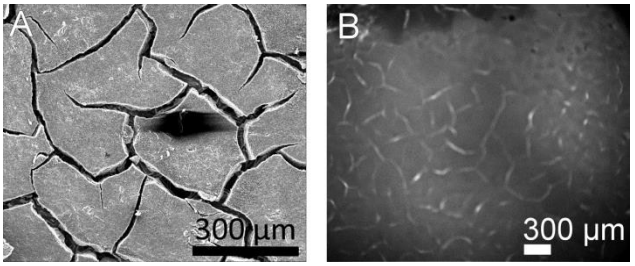

Fig. 4 A: SEM image of GDE, cracks in the active layer makes the carbon paper beneath visible, B: Optical image of fluorescence intensity after 4 s of oxygen redution at the GDE (E_{GDE} = -0.7 V) in 1 M $LiClO_4$ in DMSO

During drying, the slurry of the active carbon materials forms cracks (Fig. 4A) as commonly seen in GDE processed according to similar protocols.[25] When switching on the ORR at the GDE

by applying a potential pulse of E_{GDE} = -0.7 V, the highest fluorescence intensity after 4s reaction time is observed in the cracks (Fig. 4B). The higher fluorescence intensity in the cracks is particular obvious after switching on ORR and diminishes with time due to the diffusion of the fluorescent molecules into the solution bulk until it vanishes after 50 s of ORR. Several facts may contribute to higher fluorescent intensity inside the cracks. Firstly, the solution layer probed by the fluorescence measurement is thicker in the cracks compared to the optically opaque mesoporous carbon material of the GDE. Secondly, oxygen transport may be a limiting factor for solution-filled pores that leads to higher production of $O_2^{\bullet-}$ at those regions of the GDE facing the outer solution volume. Thirdly, $O_2^{\bullet-}$ formed in the inner pore volume may consume all the NBD-Cl inside the pore which leads to incomplete scavenging of $O_2^{\bullet-}$ may open up reaction channels for the follow-up reaction such as a further reduction step or a disproportionation.

According to Eq. (2), solid Li_2O_2 is formed during ORR. However, our previous studies[17] as well as Figs. 3 and 4 showed that also a soluble reaction product is released into the liquid electrolyte solution. In order to detect this product in tip-substrate voltammetry in a SECM configuration, the ME was positioned at a distance of 10 µm above the GDE by AC-SECM. The lower gas compartment was flushed with a mixture of 2 vol-% O_2 / 98 vol-% Ar while Ar was used to continuously purge the upper gas compartment. Figure 5 shows CVs recorded at the ME in a potential window between -1.2 V to 0.9 V with a scan rate v = 0.1 V s^{-1}. Figure 5, curve 1 shows the ME CV when the GDE was held at OCP and thus O_2 can permeate freely into the electrolyte. Therefore, the known reduction of O_2 to $O_2^{\bullet-}$ is observed at the ME at potentials negative of E_T = -0.5 V.[26, 27] No peaks appear in the anodic half-cycle because the reaction product at the ME is diffusing into the bulk solution and the amount of deposited Li_2O_2 on the ME is too small. When applying the potential of E_{GDE} = -0.7 V to the GDE, less oxygen reaches the ME because it is consumed at the GDE. Therefore, the ORR current at the ME is decreased in the potential range below E_T = -0.5 V (Fig.5, curve 2). However, two peaks appear in the positive going half-cycle that are not detected when the GDE is at OCP. The peak around E_T = -0.55 V seems to be related to the oxidation of $O_2^{\bullet-}$ ions present as dissolved compound within a diffusion layer above the macroscopic GDE. The potential of the signal close potential of the one electron oxygen reduction in the negative going half-cycle makes this assignment plausible. It also agrees with the fluorescence detection of $O_2^{\bullet-}$ in Fig. 3. The second peak appears at E_T = +0.4 V.

In our previous work we found that continuous detection of oxygen at a Pt ME in a Li^+-containing DMSO requires periodic regeneration of the Pt electrode surface because it becomes blocked with a solid reaction product in Li^+-containing electrolytes, most likely Li_2O_2. This behavior was also described by Sawyer and Roberts before.[28] A potential of 0.9 V was required to clean the electrode surface. The potential of the second oxidation signal at E_T = +0.4 V agrees with this compound and is also in line with reported potentials for Li_2O_2 oxidation in organic electrolytes.[27] Li_2O_2 may reach the ME surface in different ways. It can be deposited as a solid cover layer as a result of a disproportionation of $O_2^{\bullet-}$ according to eq. (5). Solved Li_2O_2 may diffuse from the GDE to the ME if Li_2O_2 possesses a finite solubility in DMSO. In particular, diffusive transport as an ion pair must be considered in this respect (Eq. (6)).

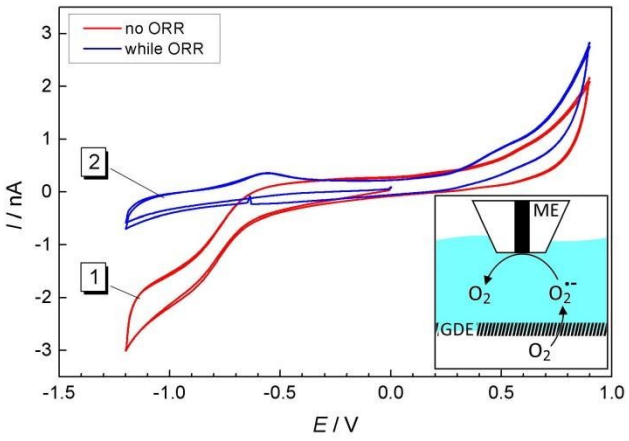

Fig. 5 CVs recorded at a ME in a distance of 10 µm distance above a GDE in 1 M $LiClO_4$ in DMSO; curve 1) GDE was held at OCP; curve 2) oxygen reduction at the GDE at E_{GDE} = -0.7 V. The scan rate was 100 mV/s. Inset: Experimental setup, oxygen from the lower gas compartment is reduced at the GDE to superoxide which diffuses towards the ME where it is oxidized/detected.

For the further investigations of the signal at E_T = +0.4 V, the potential window for the CV was restricted to 0 V < $E_T \leq$ 0.9 V. Figure 6A, curve 1 (red) shows a CV recorded at the ME while the GDE was at OCP and had not been used before for ORR. The curves show mainly capacitive currents. Afterwards the ME was left at OCP for further 15 min. Also the GDE was resting at OCP. After this incubation, another multicylce CV was recorded at the ME from which the first three cycles are shown in Fig. 6A, curve 2. Only a very small difference in the first positive-going half-cycle is noticeable compared to the measurement before the incubation time (Fig. 6A, curve 1). Because the second cycle retraces exactly the CV recorded before the incubation period, it is likely that deposits accumulated during the incubation period on the surface of the ME cause the small difference in the first half cycle of the two CVs at potentials E_T > 0.4 V in Fig. 6A. These deposits are electrochemically removed during the first positive going half-cycle.

Curve 2 in Fig. 6B shows a multicycle CV after a 15 min incubation period at which the ME and GDE was at OCP. Prior to this 15 min the GDE performed an ORR at E_{GDE} = -0.7 V for 120 s. A large peak is recorded in the first positive-going half cycle only. The absence of such a peak in subsequent cycles implies that it results from the oxidation of a compound that was accumulated during the incubation period at the surface of the ME. The dependence of this signal on a previous ORR at the GDE proves that the accumulated compound has been formed during the oxygen reduction reaction at the GDE. Since there is a solution layer of 10 µm between the GDE and the

ME, there must be a soluble (side) product of the ORR reaction in Li^+-containing DMSO at the carbon GDE. In principle this could be $O_2^{\bullet-}$ and a supersaturated Li_2O_2 solution from which it is deposited on the ME body acting as crystallization seed. The presence of $O_2^{\bullet-}$ has been proven by fluorescence microscopy (Figs. 3 and 4). Curve 2 of Fig. 5 also indicates the presence of $O_2^{\bullet-}$ in the diffusion layer above the GDE by the oxidation signal at E_T = -0.55 V. There is also a signal for the oxidation of Li_2O_2 at E_T = +0.4 V. Integration of the current between 0.4 V ≤ E_T ≤ 0.9 V in curve 2 of Fig. 6B with respect to time yield a charge of 5.0×10^{-8} As. Assuming that this charge originates from the $2e^-$ oxidation of a compact Li_2O_2 (molar mass M = 45.9 g mol^{-1}) layer with a density[29] of ρ = 2.3 g cm^{-3} leads to a layer thickness of d = 4.4 nm (Eq. (8)).

$$d = \frac{M}{nFv\rho\pi r_T^2}\int_{E_{T,1}}^{E_{T,2}} I(E_T)dE_T \qquad (8)$$

r_T the radius of the ME, F the Faraday constant, n the number of electrons transferred, v the scan rate and $I(E)$ the current measured at the ME.

Longer reduction pulses at the GDE lead to more material at the ME. However, the obtained peak splits in two components which grow differently with increasing the reduction time at the GDE (Supplementary Information, SI-1).

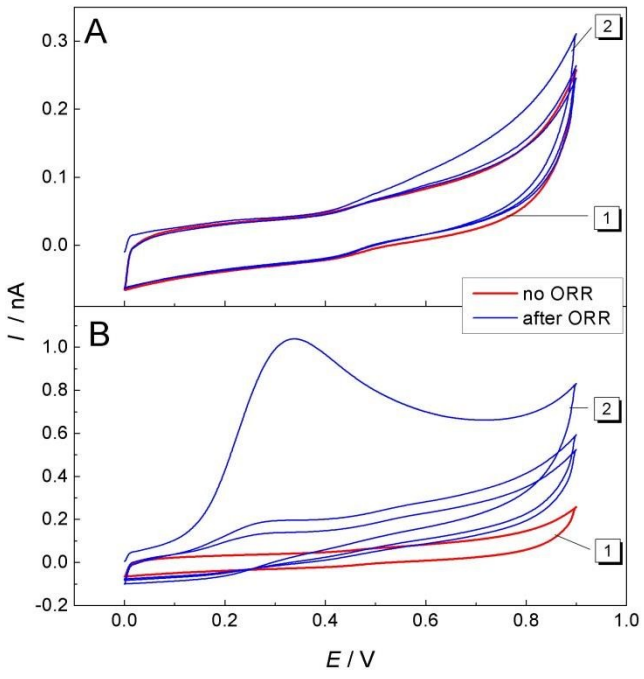

Fig. 6 CVs recorded at a ME in a distance of 10 µm distance above a GDE in 1 M $LiClO_4$ in DMSO. A) CV while the GDE is at OCP (curve 1, red) and CV after the GDE was at rest for 15 min (curve 2, blue); B) curve 1 (red) is identical to panel A, curve 1; curve 2 (blue) is the ME CV after the GDE was operated at E_{GDE} = -0.7 V for 120 s and then left 15 min at OCP. The first 3 cycles of multi-cycle CVs are shown. The scan rate was 100 mV/s.

3.2 Distance dependence of superoxide detection

Pulsed amperometric detection as described before[17] was performed at different distances of the ME to the GDE (Fig. 7). The ME was positioned 10 µm above the GDE via AC-SECM. By applying a pulse potential program to the ME, oxygen reduction and oxidation of ORR products at the ME are recorded alternatingly (Fig. 7 curve 2). A second pulse program was applied to the GDE to initiate oxygen reduction for 20 s intervals after 60 s and 180 s from the start of the measurement (Fig. 7, curve 1). The blue line in the middle panel represents the transient current at the GDE in response to a potential pulse at the GDE. In the upper panel of Fig. 7 the ME current is plotted as red dots for each acquired data point. Corresponding to the applied potential E_T the current alternates between reduction of O_2 and oxidation of a surface-bound product. The last point of each pulse is highlighted either in black squares (oxidation) or in green triangles (reduction). Those values, i.e. one data point every 10s can be used to construct images or line scans. The lines connecting the highlighted points are guides to the eyes only. Here a different approach compared to imaging or recording of linescans was selected. The double pulse experiment was repeated at different distances d from 10 µm to 90 µm with 5 µm increments. Figure 8 combines these 17 pulse experiments to false color maps where the color indicates the ME current. Figure 8A shows the last currents of each reduction pulse at the ME (Fig. 7, curve 4, green triangles) whereas Fig. 8B was constructed from the last ME current value from the oxidative cleaning pulses (e.g. Fig. 7, curve 5, black squares). The horizontal axis represents the time axis. Each pulse sequence of the ME takes 10 s (4 s reduction, 6 s oxidation). One current value for each 10 s interval is plotted in Fig. 8A and B. The vertical distance is the ME-GDE distance used in each pulse sequence.

Since the potential has to be sufficiently high for an oxidative removal of the blocking layer at the ME, E_T = +0.9 V was chosen. At this potential it is impossible to distinguish between different ORR species. Both, $O_2^{\bullet-}$ and solid Li_2O_2 deposited on the ME and dissolved Li_2O_2 may contribute to the oxidation current at the ME. Nevertheless, the effect of oxygen reduction at the GDE can be seen in both graphs. When the potential of the GDE is switched from E_{GDE} = 0 V to E_{GDE} = -0.7 V for 20 s after 60 s and 180 s to initiate ORR at the GDE, the reduction current at the ME decreases because O_2 is already consumed at the GDE (Fig. 8A). Despite the low time resolution of 10 s, one can also see that the decline of the ME current is less steep, if the ME-GDE distance is increased in agreement with the development of a macroscopic O_2 diffusion layer above the GDE. The ME current increased again when ORR stops at the GDE. The ingress of O_2 leads to diffusion layer above the GDE where the O_2 concentration decreases from the GDE towards the solution bulk when the GDE is at OCP. Because the diffusion layer above the GDE is not at steady state, the O_2 concentration change is particular steep. At distances below 25 µm the ME body shields the flux of O_2 towards the ME and this decreases the O_2 flux to the ME. This effect has been observed in sample-generation/tip-collection experiments before albeit in different contexts.[30-32]
Figure 8B shows an equivalent false color map constructed from the last point of the oxidative cleaning pulses at the ME of the *same* pulse experiments as used for Fig. 8A. Within the

time resolution of the measurement (10 s), an instantaneous increase in current during the cleaning pulses at the ME is noticeable when the GDE conducts ORR for distances of d = 10 µm and d = 15 µm. The short diffusion path for any soluble intermediate makes it possible to diffuse accross the electrolyte layer between the ME and the GDE within the time for one double pulse. When switching the GDE back to E_{GDE} = 0 V at t = 80 s and t = 200 s, the ME current does not return immediately to the value recorded immediately before the start of the reduction pulse at the GDE because the remaining $O_2^{\bullet-}$ in the solution volume between the ME and GDE constitute a reservoir that is only slowly depleted by the reaction at the ME, diffusion to the solution bulk and reaction at the GDE. The time for the oxidative currents to decline is increased with increasing working distance because the shielding of the ME with respect to the solution bulk but also the effect of a possible reaction at the GDE on the local concentration is decreased. This is evident for distances from d = 10 µm to d = 40 µm in Fig. 8B. The maximum current is shifting to later times due to the increasing diffusion length. The highest current during the cleaning pulses is observed at a distance of d = 40 µm. This phenomena can be explained by the combined action of four processes: *i*) A concentration gradient of soluble reaction products from ORR at the GDE ($O_2^{\bullet-}$, perhaps supersaturated $Li_2O_{2(solv)}$) will lead to decreasing local concentration with increasing distance to the GDE. *ii*) At short ME-GDE distances the insulating sheath of the ME hinders the diffusion of these species from the solution bulk to towards the ME.[33] *iii*) Reaction products produced directly beneath the ME during reduction pulses at the GDE can reach the ME directly without geometric hindrance by the insulating sheath of the UME. *iv*) The superoxide may undergo disproportionation reaction according to Eq. (5). This reaction is likely to be of second order. As a consequence the local concentration will initially decay very rapidly but at small concentration the reactions proceeds with a slow rate and traces of $O_2^{\bullet-}$ can exist for relatively long times as observed in Fig. 8B. Those four considerations will give us a maximum current at a certain distance, here d = 40 µm. At larger distances, the influence of the radicals from the bulk phase gain influence. At a distance of d = 75 µm another effect becomes dominating. When O_2 is reduced at the GDE, this affects the ORR current the ME only slightly because the O_2 diffusion layer at this distance is less disturbed than at shorter distances. Hence the amount of deposited Li_2O_2 does not vary as strong as at shorter distances. Consequently, less Li_2O_2 can be oxidized and the current decreases. At t = 70 s and t = 190 s the current increases again and reaches its maximum at the next ME pulse cycle. The phenomenon is due to the slightly larger diffusion coefficient of O_2 compared the $O_2^{\bullet-}$ in DMSO [28]. Data obtained at larger distances shows an increase of the influence of the O_2 concentration and a decrease of the influence of $O_2^{\bullet-}$.

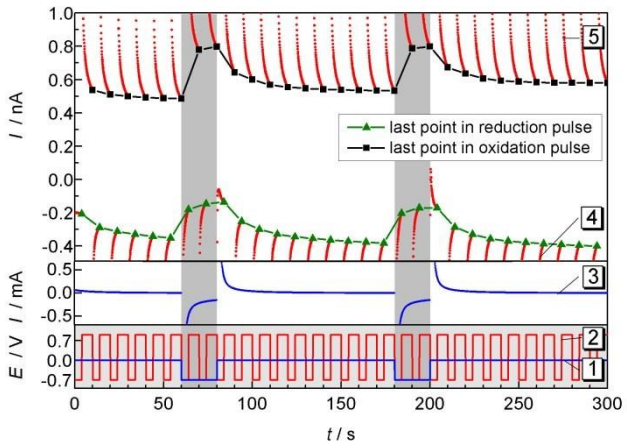

Fig. 7 ORR (4 s) and cleaning pulses at the ME (6 s) during pulsed ORR at the GDE in 1 M $LiClO_4$ in DMSO. After 60 s and 180 s oxygen is reduced at the GDE for 20 s. Lower panel: potential programs of the GDE (curve 1) and of the ME (curve 2); middle panel: current at the GDE (curve 3); upper panel: current at the ME (curve 4 and 5), the last points within each potential pulse are highlighted as green triangles (reduction) or black squares (oxidation). The solid black and green lines are guides to the eye illustrating the current trace used to construct Fig. 8A and B; d = 10 µm.

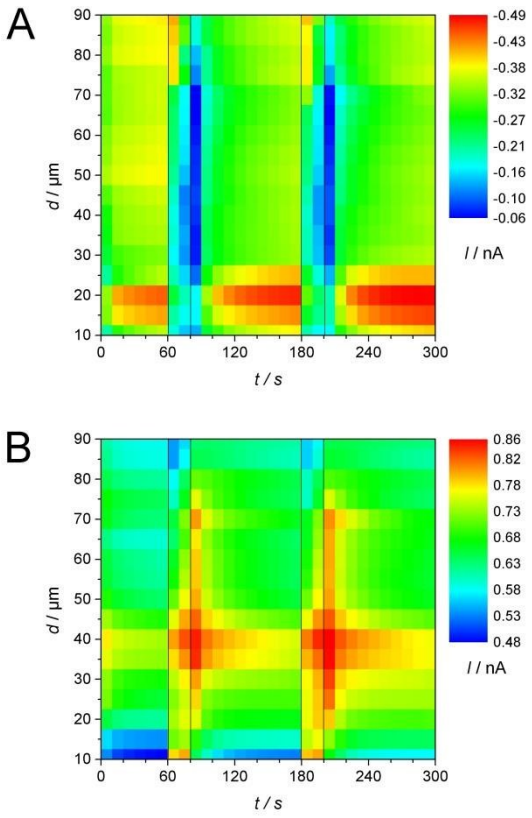

Fig. 8 False color maps constructed from 17 pulsed amperometric detections as exemplified in Fig. 7. For each amperometric recording the ME-GDE distance was incremented by 5 µm between 10 µm and 90 µm. The current values were extracted from the last points of a reduction pulse (A) or of an oxidation pulse (B) as shown in Fig. 7 and are shown here as false colors. O_2 was reduced at the GDE (E_{GDE} = -0.7 V) at t = 60 s and t = 180 s for 20 s.

4. Conclusion

In our previous work we reported the detection on an unidentified soluble species of the ORR at carbon GDE in 1 M $LiClO_4$ in DMSO,[17] i.e. not all oxygen reduction products seem to be deposited as Li_2O_2 or Li_2O at the GDE. Here we proved by detection with NBD-Cl that *soluble* $O_2^{\bullet-}$ is formed at least as an intermediate. Since the reaction with the fluorogenic compound NBD-Cl removes $O_2^{\bullet-}$ and the stable reaction product with NBD-Cl diffuses away from the GDE, no statements are possible from these measurements about the local concentration of $O_2^{\bullet-}$ above the GDE. SECM substrate-generation/tip-collection experiments were used to access the local concentration of various species during the pulses. They showed two oxidation peaks at the ME while the GDE performed ORR. Based on the similarity of the peak potential to the peak for $O_2^{\bullet-}$ generation at the ME, one peak is assigned to the oxidation of the $O_2^{\bullet-}$ radical. The second peak rises from oxidation of a solid lithium-oxygen species, most probably Li_2O_2 deposited on the surface of the ME. It could be removed by only one half-cycle of a CV. No hints for further dissolved species were found.

By combining several pulsed potential experiments to one false color map it was possible to visualize the correlation between ME-GDE distance and local O_2 concentration and $O_2^{\bullet-}$ concentration, respectively. The influence of the $O_2^{\bullet-}$ diminishes for distances larger than d = 75 µm.

The occurrence of soluble reactive oxygen species during charging *and* discharging reactions in Li-oxygen cells will not only cause decomposition reactions with solvent and electrolyte constituents but may also lead to the attack on solid components that are spatially separated from the GDE. Deposition of lithium oxides may further impact passivation layers and thus the kinetics of various interfacial reactions. Means of controlling the generation of superoxide and/or its further reaction close to the GDE may represent a sensible way of overcoming the obstacles described above.

Acknowledgement

The study is funded by the Lower Saxony Ministry of Science and Culture. S.D. gratefully acknowledges a PhD study grant from German Academic Exchange Office (DAAD).

References

1. M. Balaish, A. Kraytsberg and Y. Ein-Eli, *Phys. Chem. Chem. Phys.*, 2014, **16**, 2801-2822.
2. S. A. Freunberger, Y. Chen, N. E. Drewett, L. J. Hardwick, F. Bardé and P. G. Bruce, *Angew. Chem. Int. Ed.*, 2011, **50**, 8609-8613.
3. J. M. García, H. W. Horn and J. E. Rice, *J. Phys. Chem. Lett.*, 2015, **6**, 1795-1799.
4. D. Zhu, L. Zhang, M. Song, X. Wang, J. Mei, L. M. Lau and Y. Chen, *J. Solid State Electrochem.*, 2013, **17**, 2865-2870.
5. S. A. Freunberger, Y. Chen, Z. Peng, J. M. Griffin, L. J. Hardwick, F. Bardé, P. Novák and P. G. Bruce, *J. Am. Chem. Soc.*, 2011, **133**, 8040-8047.
6. N. Mozhzhukhina, L. P. Méndez De Leo and E. J. Calvo, *J. Phys. Chem. C*, 2013, **117**, 18375-18380.
7. B. D. McCloskey, D. S. Bethune, R. M. Shelby, G. Girishkumar and A. C. Luntz, *J. Phys. Chem. Lett.*, 2011, **2**, 1161–1166-1161–1166.
8. C. J. Bondue, A. A. Abd-El-Latif, P. Hegemann and H. Baltruschat, *J. Electrochem. Soc.*, 2015, **162**, A479-A487.
9. V. S. Bryantsev, V. Giordani, W. Walker, M. Blanco, S. Zecevic, K. Sasaki, J. Uddin, D. Addison and G. V. Chase, *J. Phys. Chem. A*, 2011, **115**, 12399-12409.
10. V. S. Bryantsev, J. Uddin, V. Giordani, W. Walker, D. Addison and G. V. Chase, *J. Electrochem. Soc.*, 2013, **160**, A160-A171.
11. A. D. Goolsby and D. T. Sawyer, *Anal. Chem.*, 1968, **40**, 83-86.
12. C. P. Andrieux, P. Hapiot and J. M. Saveant, *J. Am. Chem. Soc.*, 1987, **109**, 3768-3775.
13. E. S. Boyd and G. K. Druschel, *Appl. Environ. Microbiol.*, 2013, **79**, 2061-2068.
14. G. P. Haight and K. M. Rahmoeller, *Polyhedron*, 1986, **5**, 507-509.
15. Z. Peng, Y. Chen, P. G. Bruce and Y. Xu, *Angew. Chem. Int. Ed.*, 2015, **54**, 8165-8168.
16. C. Zhang, F.-R. F. Fan and A. J. Bard, *J. Am. Chem. Soc.*, 2009, **131**, 177-181.
17. P. Schwager, D. Fenske and G. Wittstock, *J. Electroanal. Chem.*, 2015, **740**, 82-87.
18. C. Nunes Kirchner, K. H. Hallmeier, R. Szargan, T. Raschke, C. Radehaus and G. Wittstock, *Electroanal.*, 2007, **19**, 1023-1031.
19. K. Eckhard and W. Schuhmann, *Analyst*, 2008, **133**, 1486-1497.
20. D. M. Osbourn, R. H. Sanger and P. J. S. Smith, *Anal. Chem.*, 2005, **77**, 6999-7004.
21. B. R. Horrocks, D. Schmidtke, A. Heller and A. J. Bard, *Anal. Chem.*, 1993, **65**, 3605-3614.
22. M. V. Mirkin, F.-R. F. Fan and A. J. Bard, *J. Electroanal. Chem.*, 1992, **328**, 47-62.
23. G. Bartosz, *Clin. Chim. Acta*, 2006, **368**, 53-76.
24. J. Burns, W. Cooper, J. Ferry, D. W. King, B. DiMento, K. McNeill, C. Miller, W. Miller, B. Peake, S. Rusak, A. Rose and T. D. Waite, *Aquat. Sci.*, 2012, **74**, 683-734.
25. R. Zeis, *Beilstein J. Nanotechnol.*, 2015, **6**, 68-83.
26. I. Gunasekara, S. Mukerjee, E. J. Plichta, M. A. Hendrickson and K. M. Abraham, *J. Electrochem. Soc.*, 2014, **161**, A381-A392.
27. C. O. Laoire, S. Mukerjee, K. M. Abraham, E. J. Plichta and M. A. Hendrickson, *J. Phys. Chem. C*, 2010, **114**, 9178-9186.
28. D. T. Sawyer and J. L. Roberts, *J. Electroanal. Chem.*, 1966, **12**, 90-101.
29. W. M. Haynes and D. R. Lide, *CRC Handbook of Chemistry and Physics : A Ready-reference Book of Chemical and Physical Data*, CRS Press, Boca Raton, 2014.
30. B. R. Horrocks, M. V. Mirkin, D. T. Pierce, A. J. Bard, G. Nagy and K. Toth, *Anal. Chem.*, 1993, **65**, 1213-1224.
31. O. Sklyar, M. Träuble, C. Zhao and G. Wittstock, *J. Phys. Chem. B*, 2006, **110**, 15869-15877.
32. L. Stoica, S. Neugebauer and W. Schuhmann, *Adv. Biochem. Eng./Biotechnol.*, 2008, **109**, 455-492.
33. R. Cornut and C. Lefrou, *J. Electroanal. Chem.*, 2008, **621**, 178-184.

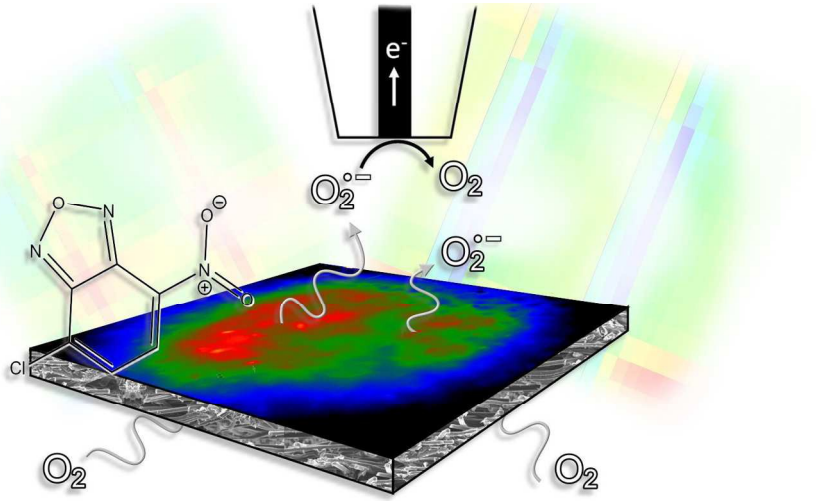

666x333mm (72 x 72 DPI)